ORIGINAL PAPER

C. Scheibner · J. Kuss · A. M. Marzouk

Slope sediments of a Paleocene ramp-to-basin transition in NE Egypt

Abstract Sedimentary structures, microfacies and stratigraphy of a late Paleocene ramp-to-basin transition have been studied in the Galala Mountains in the northern part of the Eastern Desert of Egypt. Three phases of ramp progradation were observed. During non-progradation hemipelagic sediments were intercalated. These progradational phases are indicated by mass-transport deposits of glides slumps and debris flows which came from different directions except from the south. At least two of these mass-transport deposits may reflect deposition during sea-level lowstands, whereas the hemipelagic intercalations indicate transgressive phases. Microfacies analysis provided evidence of a change in the origin of the debris flow deposits. They show a transition from a basinal-to-outer-ramp setting to a middle-to-inner-ramp setting and a change in organism distribution. While coralline red algae prevailed on the inner ramp in the Selandian to Thanetian, nummulitids dominated in the late Thanetian.

Key words Middle to Late Paleocene · Glides · Slumps · Debris flows · Microfacies analysis · Algal shoals · Nummulitidae shoals

Introduction

The area of the Galala mountains (Eastern Desert, Egypt) has been the focus of numerous studies mostly dealing with biostratigraphy and lithostratigraphy (Is-

C. Scheibner (✉) · J. Kuss
Department of Geology, Bremen University, Fachbereich 5,
P.O. Box 330440, D-28334 Bremen, Germany
e-mail: scheibne@uni-bremen.de
Fax: +0421-2184515

A. M. Marzouk
Department of Geology, Faculty of Science, Tanta University,
ET-31527 Tanta Egypt

mail and Abdallah 1966; Abdou et al. 1969; Abdel Kireem and Abdou 1979; Strougo et al. 1992; Faris 1994). Only a few studies have dealt with the overall architecture of the depositional system (Bandel and Kuss 1987; Kuss and Leppig 1989; Kulbrok 1996; Gietl 1998; J. Kuss et al., submitted). These authors propose a stuctural high during late Cretaceous times, situated at the central and southern parts of the North Galala including the Wadi Araba area to the south. Late Cretaceous slope deposits of the mid-outer ramp are exposed at the monastery of St. Anthony (Fig. 1); however, they are not present further south at the monastery of St. Paul where only their basinal equivalents occur (Kulbrok and Kuss 1995). Ramp progradation continued during the Paleogene. The first ramp-derived allochthonous sediments were transported during the Selandian from northerly directions to the St. Paul area. The sections studied, west of the monastery of St. Paul, represent a segment of a ramp to basin transition within that southward-prograding ramp system.

This paper concentrates on an excellent, continuous outcrop near the monastery of St. Paul, 360 m wide and 50 m high, including a massive layer (20 m) composed of various units of mass-transport sediments (Figs. 1, 2). They exhibit multiple transitions between glides and debris flows (DFs), composed mainly of carbonates with only minor contents of quartz. Thin-section analysis of allochthonous carbonates indicates a wide spectrum of components originally formed in different environments of the Paleogene carbonate ramp situated further north. Many limestones within the different allochthonous units are comparable to shallow-water autochthonous ramp environments described previously by Gietl (1998). Moreover, we discuss various stages of ramp progradation during the late Paleocene.

Fig. 1 Topography of the Galala Mountains, Eastern Desert, Egypt, with inset maps of Egypt and the vicinity of the monastery St. Paul. Sections are indicated

Geological setting

During Maastrichtian to early Eocene times, a south-dipping carbonate ramp evolved in the northern parts of the Eastern Desert of Egypt (Galala Heights; Fig. 1). Predominantly carbonate sediments were deposited along an E–W running tectonically induced uplift that covered parts of the present North Galala and Wadi Araba. This uplift represents the southern-most area affected by the Syrian Arc fold belt (Mous-tafa 1995). It was formed as a consequence of the clos-ing Tethys since Turonian times (Lüning et al. 1998).

The lower to upper Paleocene strata in the area of St. Paul reflect a transition from distal ramp settings, with basinal hemipelagic sediments, to settings in-fluenced by carbonate mass-transport deposits and shallow-water limestones. The Danian to Selandian (Planktic Foraminifers P1–P3 biochrons) basinal marls overlie upper Cretaceous (Maastrichtian) basinal chalks with marly intercalations of up to 12 cm thick-ness, whereas the chalky layers reach maximum thick-nesses of 75 cm. In the upper part of the upper Maas-trichtian succession, a few thin black shale intervals are intercalated.

A biostratigraphically continuous record across the K/T boundary is well documented in most sections of the St. Paul area, where sediments of the upper Maas-trichtian calcareous nannoplankton *Micula prinsii* zone are overlain by Paleocene strata of the planktic foraminifer P1a zone (middle part of calcareous nan-noplankton zone NP1, Strougo et al. 1992; Faris 1995).

Marls prevail up to zone P3b (Fig. 2) and are dis-conformably overlain by limestones. Carbonate depo-sition was interrupted by two prominent marly inter-calations during late NP5 and NP6 (Figs. 3, 4).
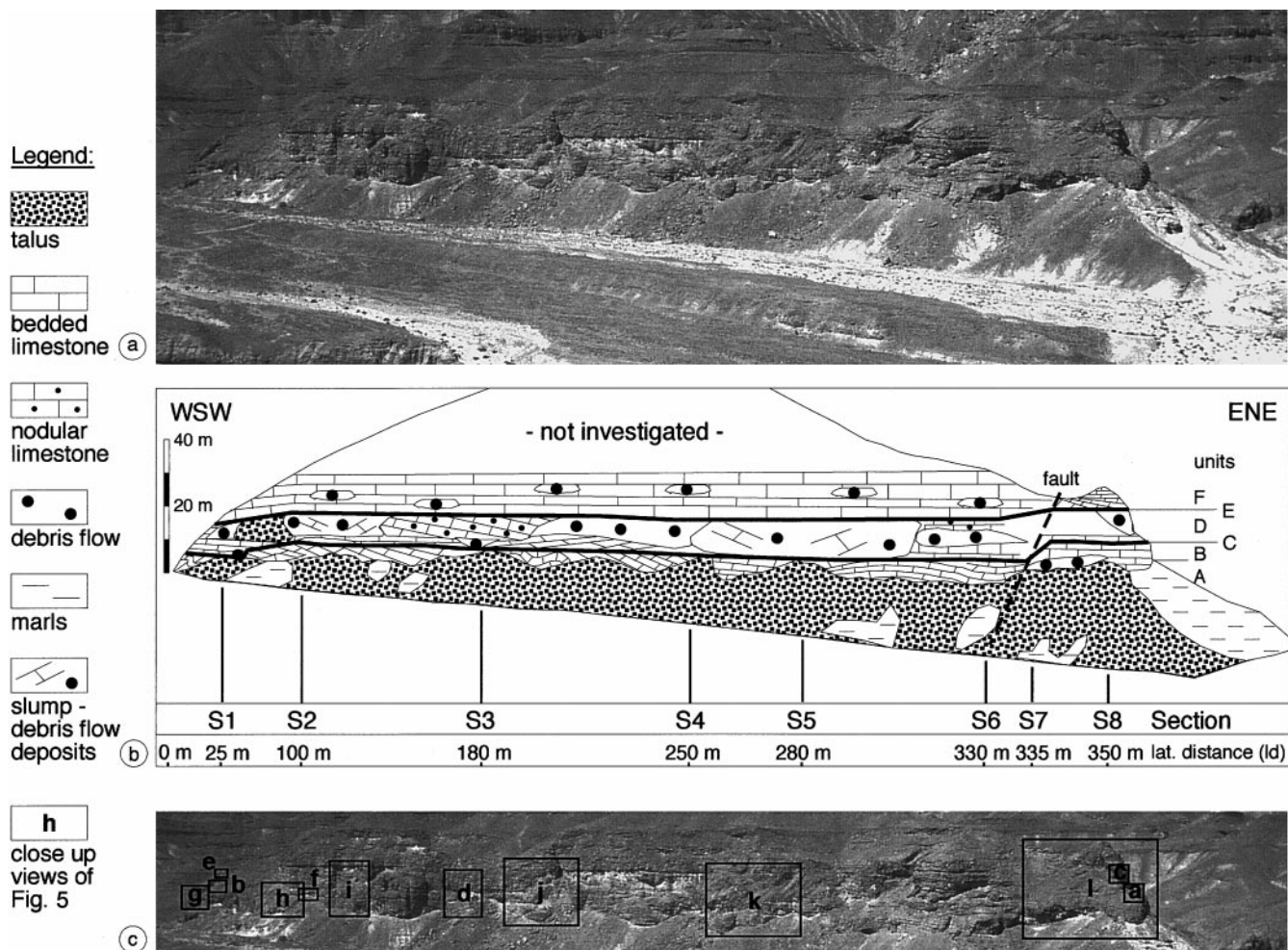
Fig. 2 **a** Investigated outcrop. **b** Sketch of outcrop with sedimentological features and location of sections. **c** Outcrop with location of close-up photographs shown in Fig. 5

Few shallow-water communities of organic buildups recovered from the late Maastrichtian to early Paleocene biotic crisis (Schuster 1996). Diversity of carbonate communities began to increase again during the late Paleocene. Organic buildups were composed mainly of corals and red algae, although bryozoans are also reported locally (Bryan 1991; Vecsei and Moussavian 1997). The Eocene, however, was a time when larger foraminifers (mainly *nummulites*) thrived in shallow-water environments (Aigner 1983). An overview of the paleoecology of reefal foraminifers and algae in the Cenozoic is given by Ghose (1977).

Materials and methods

The ramp to basin transition was studied along a roughly WSW–ENE striking wadi ridge within the foothills south of the rising escarpment of the South Galala heights (Fig. 1) situated 2.5 km west of the monastery of St. Paul (E 32°31,288′; N 28°50,718′). The outcrop was subdivided into six distinct lithostratigraphic units.

The study is based on a detailed facies analysis (macro- and microscale) of eight vertical sections (S1–S8), taken along a lateral profile. Eighty-seven limestone samples were studied through thin-section analyses and 42 marly-shale samples for micropalaeontological studies (Fig. 4). A detailed mapping of all sedimentological and structural features along the outcrop was supported by a photomosaic (Figs. 2, 5). Additionally, one parallel section (S9) was taken approximately 1 km to the SE of the profile presented here (Fig. 1) and covers the uppermost Cretaceous to lower Eocene succession. Sixty washed samples and 15 thin-section samples were studied from this section and yield supporting data but are discussed in a forthcoming paper by J. Kuss et al. (submitted).

Biostratigraphy

The biostratigraphic framework is based on both planktic and larger foraminifers, and calcareous nannoplankton. The biozonal and chronostratigraphic

711

Fig. 3 Paleocene to Eocene time scale. The time (Ma), epoch, age and planktonic foraminifers zonation are from Berggren et al. (1995). Calcareous nannoplankton zonation is from Martini (1971), the shallow benthic zonation is from Serra-Kiel et al. (1998) and the larger foraminifer zonation is from Hottinger et al. (1964) and Gietl (1998). The *broad grey band* reflects the current opinion on the position of the Paleocene/ Eocene boundary. The *black rectangle* marks the stratigraphic interval investigated in sections *S1–S8*. Within the *rectangle* the units described and cycle boundaries are marked. Comparisons of cycle boundaries are based on absolute ages. Mismatches are due to different biostratigraphic concepts used by the authors

Time (Ma.)	Epoch	Age	P Zone (Berggren et al. 1995)	NP Zone (Martini 1971)	SBZ (Serra-Kiel et al. 1998)	larger foraminifers (Hottinger, Lehmann & Schaub 1964; Gietl 1998)	units	This work	Lüning et al. (1998)	Hardenbol et al. (1999)
50	Eocene	Ypresian	P8	NP13	SBZ11	A.(A.) dainellii				
			P7	NP12	SBZ10	A.(A.) schwageri				
			P6 b	NP11	SBZ9	A.(A.) trempina				
					SBZ8	A.(A.) corbarica				
			P6 a	NP10	SBZ7	A.(A.) moussoulensis				
55			P5	NP9	SBZ6	A.(A.) ellipsoidalis				
					SBZ5	A.(A.) cucumiformis				
	Late Paleocene	Thanetian	P4 c		SBZ4	A.(G.) levis	F	ThGal1	ThSin5	Th5 / Th4
			P4 b	NP8	SBZ3	A.(G.) primaeva				Th3
			P4 a	NP7 / NP6			E		ThSin4	Th2
		Selandian		NP5			D / C / B	SelGal? / SelGal2	ThSin3 / ThSin2	Th1
60			P3 b		SBZ2		A			
			P3 a	NP4					ThSin1	Sel1
	Early Paleocene	Danian	P2							
			P1 c	NP3	SBZ1					
			P1 b	NP2						
65			Pa & P0 a	NP1						

standards of Berggren et al. (1995) and Olsson et al. (1999) are used for planktic foraminifers, Martini (1971) for calcareous nannoplankton biozonation, and Hottinger et al. (1964), Serra-Kiel et al. (1998), and Gietl (1998) for larger foraminifers biozonation (Fig. 3).

Planktic foraminifers

Planktic foraminifers were found in marls of Units A, B, C and E. A well-preserved assemblage of *Acarinina strabocella, Morozovella angulata, M. conicotruncata, Igorina albeari, Globanomalina chapmani, Gl. haunsbergensis* occurs in Unit A. *Globanomalina pseudomenardii, Acarinina subsphaerica* and *A. mackanni* were not found in this unit, indicating biozone P3b. Forms morphologically similar to *M. acuta* were found as well but may belong to *M. conicotruncata*. Two samples of Unit B contain poorly preserved planktics, which could not support a biostratigraphic assessment.

A similar assemblage of planktic foraminifers as in Unit A was observed in Unit C. Moreover, the first specimens of *M. velascoensis* were found, which could be attributed to biozone P4 (Fig. 4).

Unit E was also attributed to biozone P4, suggested by typical *M. velascoensis* with well-pronounced decoration, and the first occurrence of *Acarinina* sp. The index fossil *G. pseudomenardii* was not found. Luger (1985) indicated that *G. pseudomenardii* is seldom found in Egypt.

Larger foraminifers

Several index species were identified in thin sections: *Glomalveolina* sp., *Hottingerina lukasi* and the two conical species *Fallotella kochanskae persica* and *F. alavensis*. According to Drobne (1975), *H. lukasi* ranges within the *A. (G.) primaeva* biozone in Slovenia; however, White (1994) demonstrated this species ranging from *A. (G.) primaeva* to *A. (A.) ellipsoidalis* zones in Oman. Serra-Kiel et al. (1998) described it as index fossil of shallow benthic zone SBZ 4. Gietl (1998) and Kuss and Leppig (1989) described *H. lukasi* in the Galala Mountains from the *A. (G.) levis* biozone. *Fallotella alavensis* was found by Leppig (1987) in Spain coinciding with the *A. (G.) primaeva* biozone, and according to Hottinger and Drobne (1980) and Serra-Kiel (1998) this species is restricted to the *A. (G.) primaeva* biozone. The same is true for
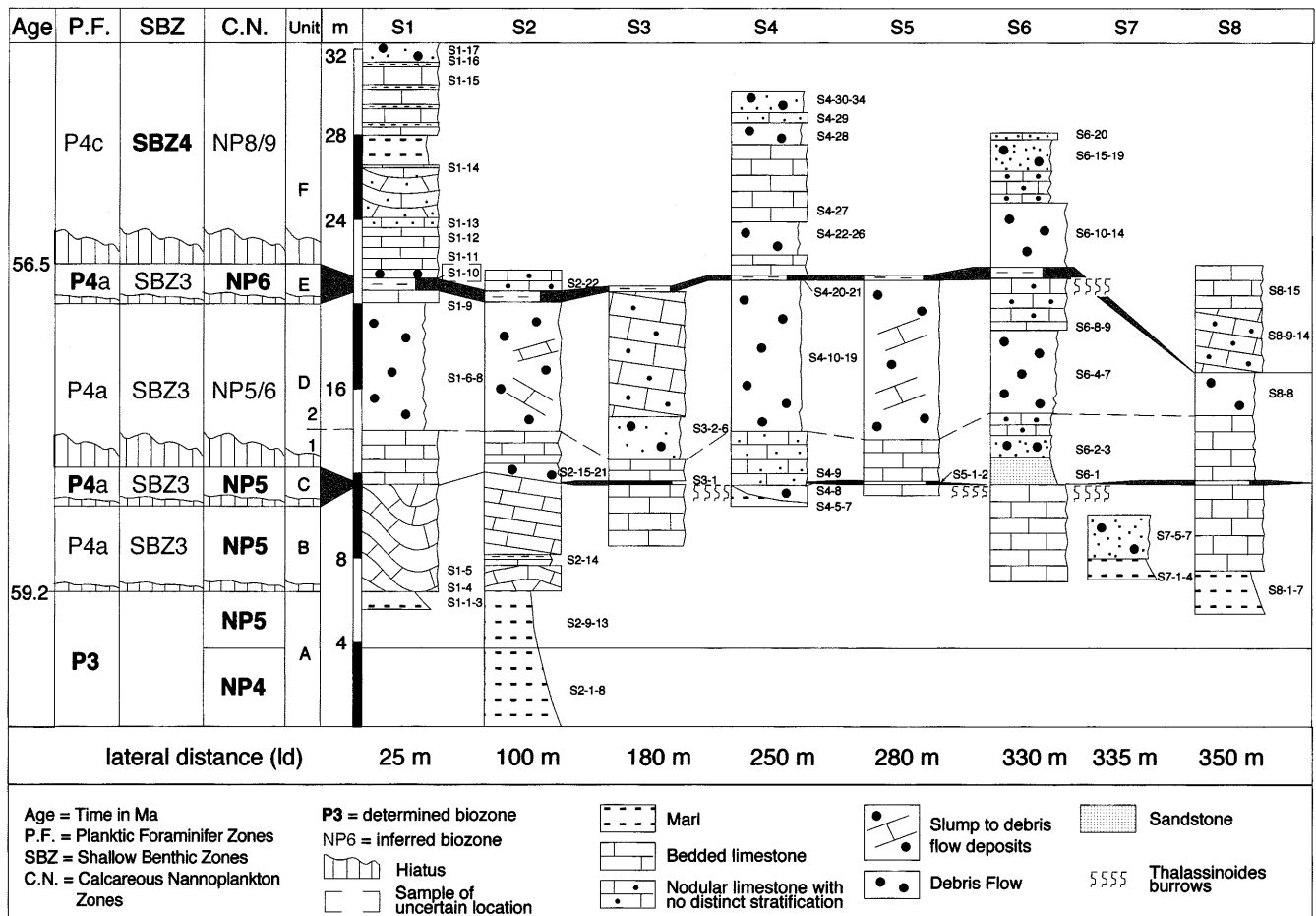
Fig. 4 Stratigraphic correlation of sections S1–S8 with their typical sedimentological features. Sample numbers are indicated

F. kochanskae persica (Hottinger and Drobne 1980). In contrast, Gietl (1998) and Kuss and Leppig (1989) found this species in the *A. (G.) levis* biozone from the Galala Mountains. On the basis of this classification, the association of *H. lukasi, F. kochanskae persica, F. alavensis, Mis. rhomboidea*, Discocyclinidae, *Broeckinella, A (G.) dachelensis, Ranikothalia* and *Archeolithothamnium* has been used to define the *A. (G.) levis* biozone, coinciding with SBZ 4 of Serra-Kiel et al. (1998).

Small larger foraminifers were also found within the hemipelagic marls of Unit E.

Fig. 5a–l Photographs (left side or upper side) and illustrated sketchs (right side or lower side) of close-ups. For location and legend of close-ups see Fig. 2. Scale is in the *lower right corner* of the photographs. The *letters* within the sketches indicate the units present. The different types of debris flows (DF) present are illustrated in **a–c**. **a** Debris flow 1a, with very small clasts of approximately 1 cm, is present in one DF east of section S8. **b** Debris flow 1 with heterogeneous size distribution ranging between DF 1a and DF 1b. This is the most common DF type. **c** DF 1b with very large clasts of 25–50 cm is present in one DF in section S8. **d–l** Close-ups of the outcrop. **d** In contrast to all other DFs which are shaped convex-upward, this one is shaped convex-downward. Probably it was deposited within a channel. **e** Erosional contact of hemipelagic marly chalks of Unit E and a debris flow of Unit F (profile S1). **f** Typical convex-upward-shaped DF. The surrounding strata show onlap structures. **g** Western end of lateral profile. Here Unit B is composed of heavily slumped beds which are disconformably overlain by Unit D. The more or less horizontal carbonate layers of Unit D1 are overlain on the left by a massive slightly layered nodular limestone and on the right by a DF (for detail see Fig. 5b). **h** Generally east-dipping beds of Unit B. Note the wavy bed thinning to the left. Here one of the two DFs within Unit D1 is seen. The horizontal layers of D1 are onlapping Unit B. On top a typical slump to DF deposit is visible. **i** The contrast of the east-dipping beds of Unit B (20°) and the west-dipping, partly thinning beds of Unit D1 is clearly visible. The top is composed of slump to debris flow deposits and a debris flow. **j** Onlap pattern of massive, slightly bedded nodular limestone on a debris flow in Unit D2. Note the slumps in Units B and D1. The hemipelagic marly chalk deposits of Unit E clearly separate the shallower deposits of Units D and F. **k** Nearly horizontal layers of Unit B are overlain by a slump to DF. Again Unit E separates Units D and F. **l** The eastern end of the lateral profile. A fault and debris on the left side make the correlation to the rest of the profile difficult. Note the debris flow in Unit B with typical onlap structures of surrounding sediments. The DF of Unit D is characterised by DF type 1b with large clasts. For detail see Fig. 5c. Unit F is composed of slightly layered nodular limestones with changing inclination

e
20 cm

f
3 m

g
3 m

h
5 m

i

5 m

j

5 m

k

5 m

l

5 m
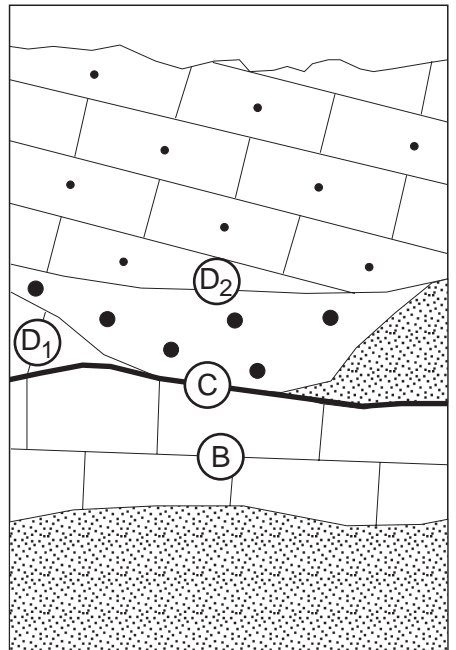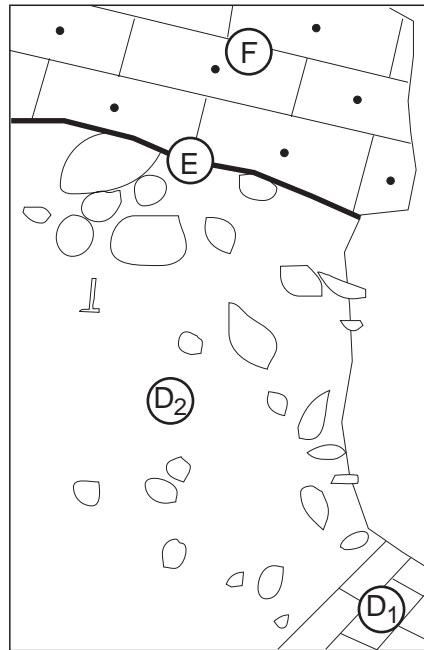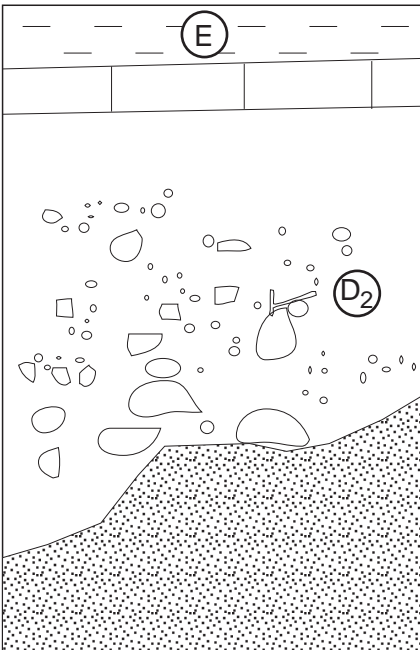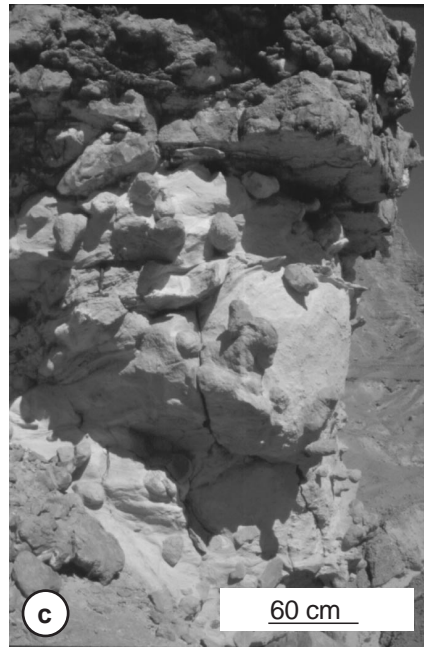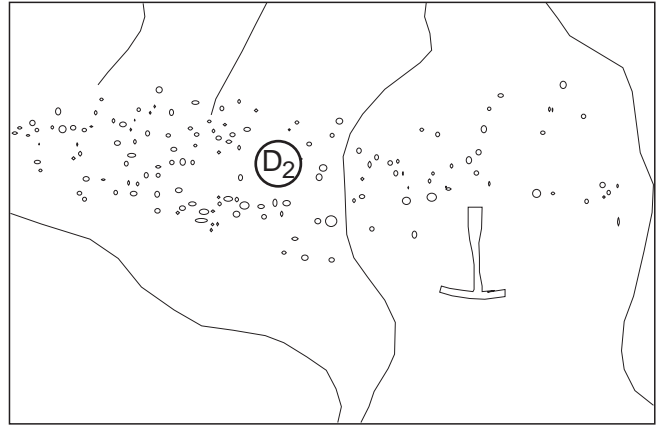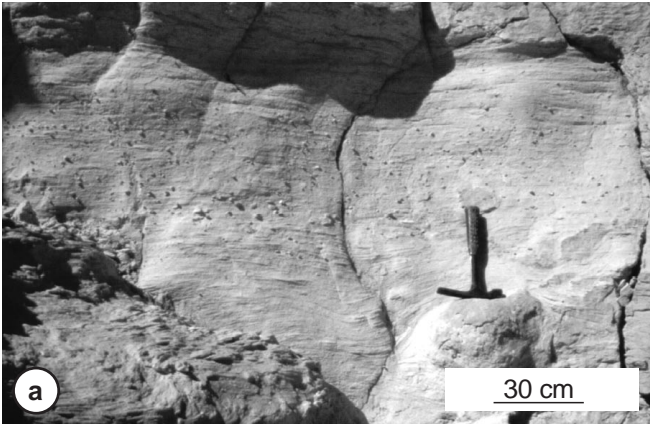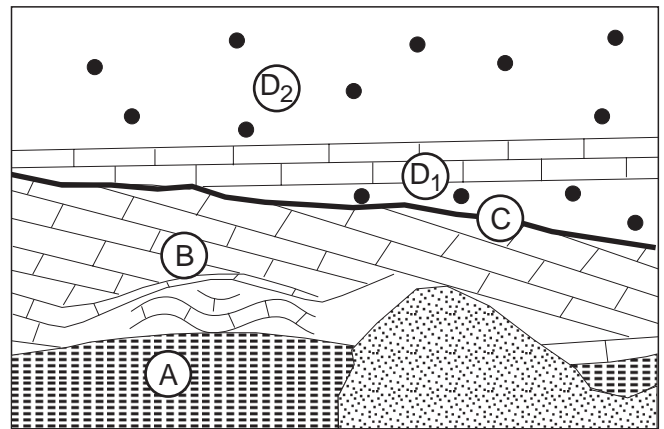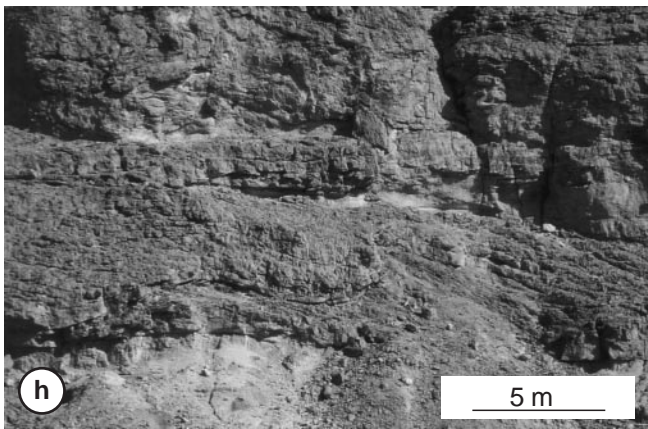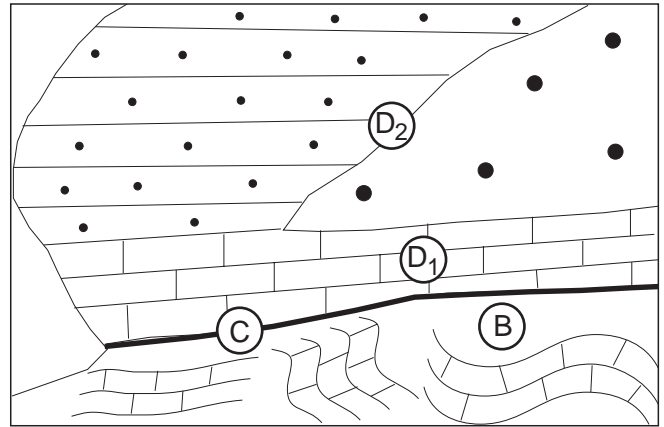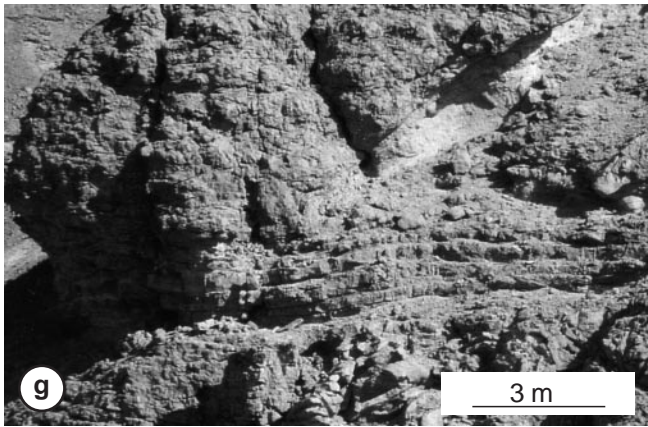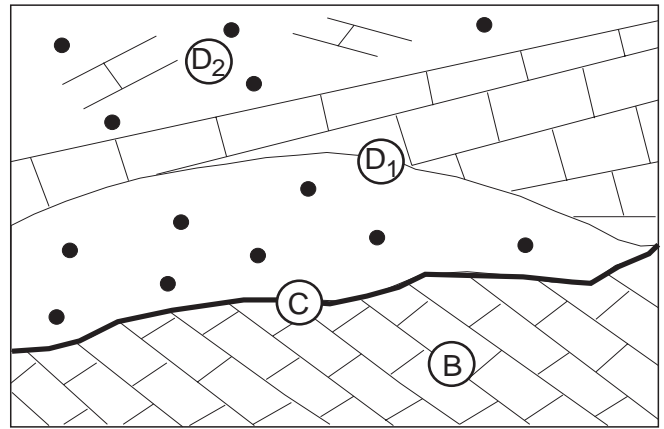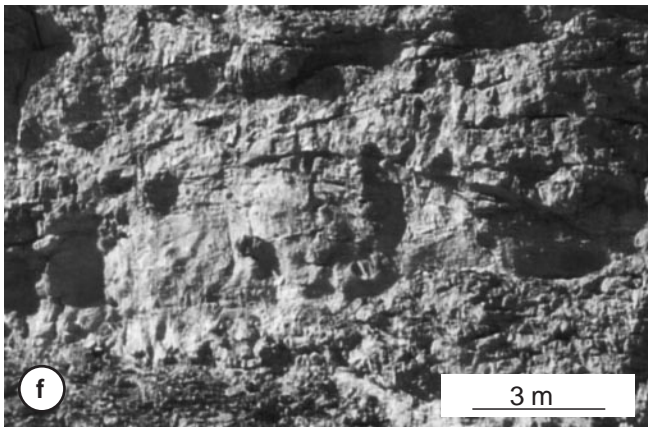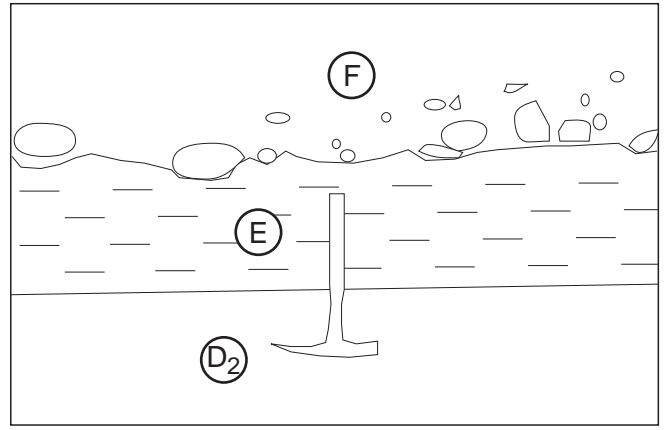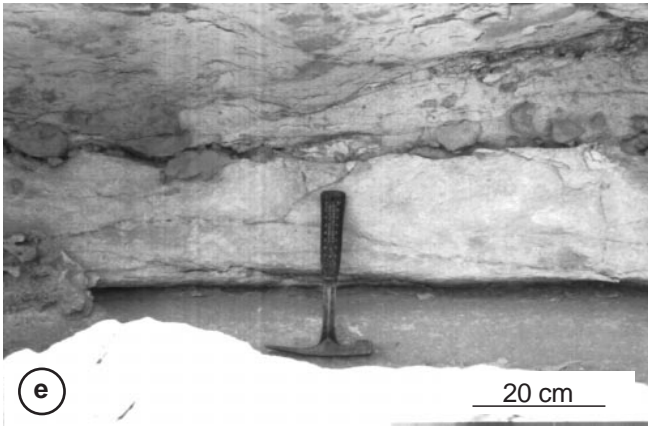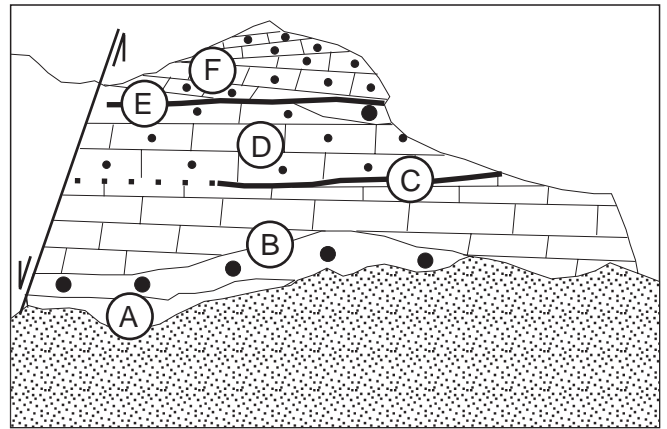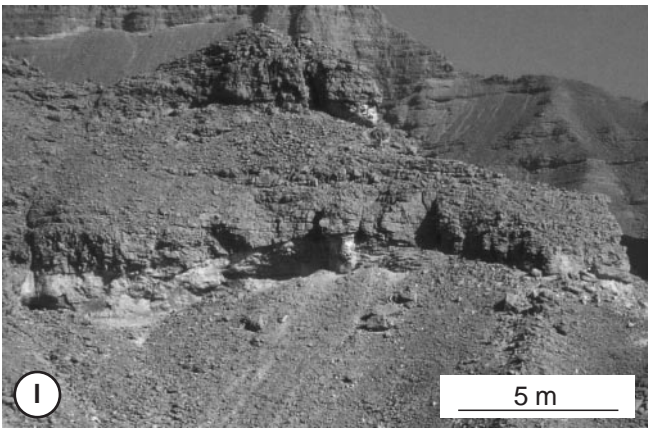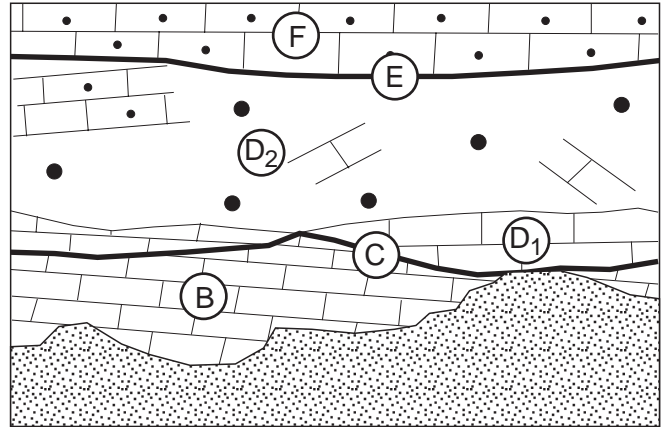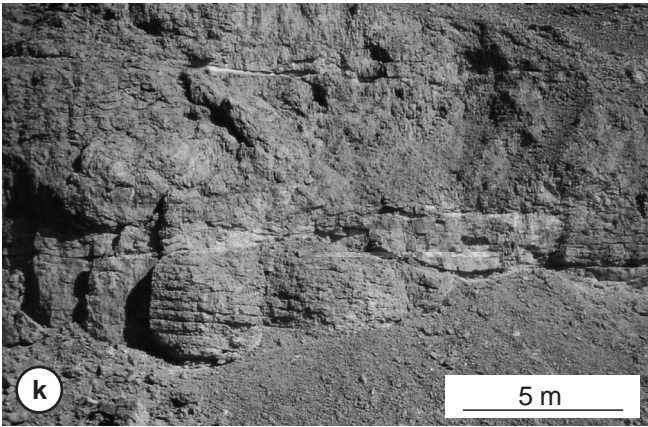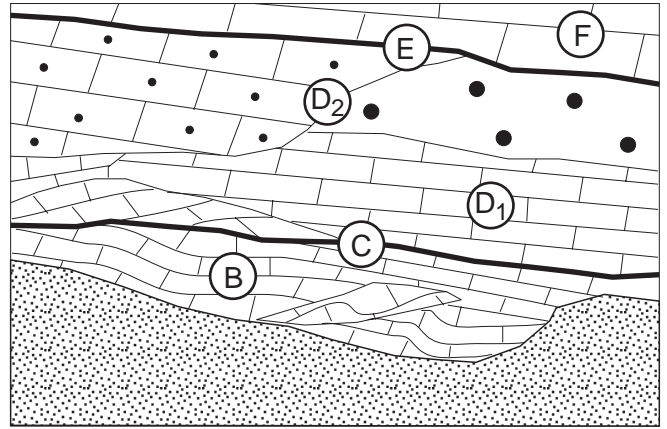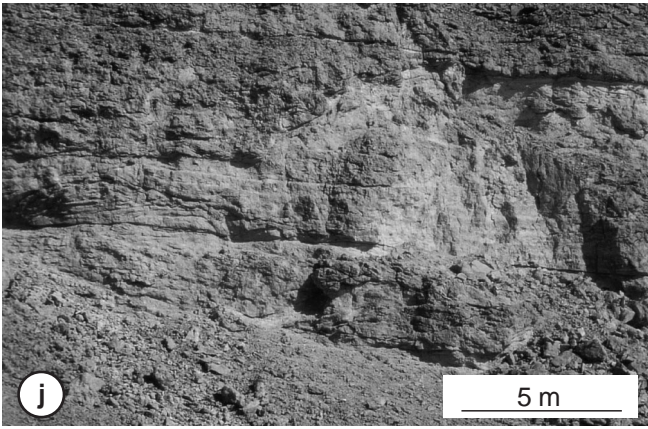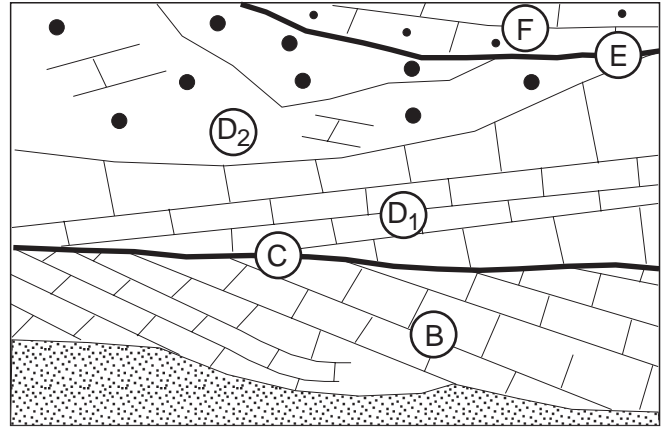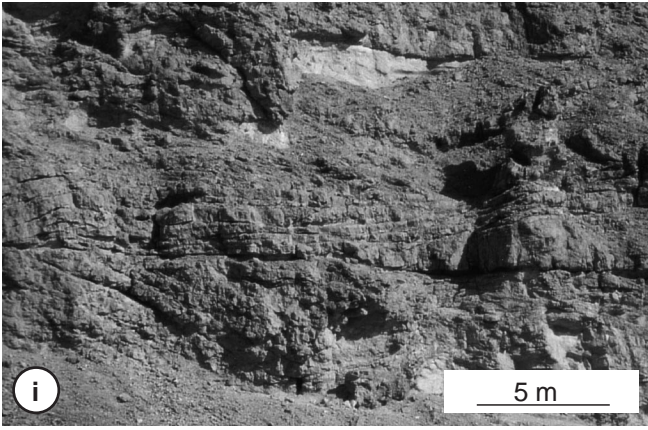
Benthic foraminifers

Whereas the benthic foraminifers of Unit A indicate a position on the deeper shelf, the samples of Units C and E contain a mixture of autochthonuous deeper (mixed Midway and Velasco Fauna, indicating a water depth of ca. 500 m) and allochthonous shallower shelf forms (Speijer 1994; R.P. Speijer pers. commun.).

Calcareous nannoplankton

Well-preserved microfloras have been identified in marls of Units A, B, C and E. Unit A was attributed to biozones NP4 (S2-1 to 8) with *Markalius inversus, Chiasmolithus tenius, Ellipsolithus macellus* (index form) and *Coccolithus pelagicus*. Units B and C have been attributed to NP5 (Fig. 4). NP5 (S1-1 to 3; S2-9 to 13; S4-5 to 7; S7-1 to 4; and S8-1 to 7) is characterised by the above mentioned species and *Fasciculithus tympaniformis* (index form), *F. janii, F. bitectus* and *Chiasmolithus consuetus*. Samples S4-20 and S4-21 of Unit E hold specimens of NP6 with the index form *Heliolithus kleinpellii*.

Lithostratigraphic units

Unit A

Unit A (thickness 5–10 m) consists of marls at the base which are of early to early late Paleocene (P1–P3) age disconformably overlain by limestones of Unit B. The sharp contact between both units, which is often covered by alluvial gravel (Figs. 2a,b), is well exposed in sections S1, S2, S8 and S9. Following the contact laterally from S1 in the west to S8 in the east, its erosive character becomes obvious: several incisions of Unit B into the soft lithologies of Unit A form a conspicuous large-scale undulating boundary along the profile (Fig. 2).

Unit B

Unit B (thickness 4–6 m) is characterised by hard, massive carbonates with various textural characteristics. Peloidal micrites prevail together with a varying degree of quartz. The latter is also frequent in washed samples (S1-5 and S2-14).

The carbonates include undisturbed horizontally to eastward-dipping bedding planes, glides and slumps. The intensity of disturbance within this unit decreases from west to east. At the western end of the profile (lateral distance, LD = 1–10 m; Fig. 2), a chaotic melange occurs with only few slumped beds that exhibit an S-shape. Next to this, an area of slumped beds occurs that are still in original sedimentary contact (LD 15 m, Fig. 5g). A little further to the east (ld 30 m), no obvious slumps occur but the beds dip at a maximum angle of 20° to the east. Dipping is best visible in the upper parts of Unit B due to its constant bed thickness. But a few basal beds exhibit changing thicknesses (Fig. 5h). Here, the younger limestone beds clearly show overlapping patterns. Further to the east, slumping ceases (LD 85 m) and the strata dip to the east with less and less inclination. East of LD 270 m (Fig. 2), no overlapping is visible but all beds have a smooth waveform appearence. Abundant *Thalassinoides* burrows were found at the top of Unit B in sections S3, S5 and S6 (Fig. 4).

Unit B is composed mainly of glides and slumps except one DF at the easternmost part of the profile between sections S7 and S8 (Figs. 2b, 5l). Prather et al. (1998) classified slope deposits from the Gulf of Mexico on the basis of seismic facies; their facies A+ Bl of chaotic rotated slump blocks exhibit similar characteristics of the slumps, submarine slides and DF described here.

Unit C

Unit C (thickness 5–8 cm) consists of a few-centimetres-thick marly intercalation exposed in sections S3 and S5 only. Units B and D overlie one another disconformably in all other sections without exposing Unit C. The correlation of Unit C with a 20-cm-thick chalk layer in section S8 is based on lithostratigraphy only, and could not be confirmed due to a fault and gravel cover between sections S7 and S8 (Fig. 5l).

Unit D

Unit D (thickness ~10 m) forms a steep cliff and allows detailed mapping of the internal sedimentological architecture based on both, field observations and the use of a photomosaic. The prevailing DFs and slump deposits in the upper part of the unit (D2) conformably overlie nearly horizontally bedded, slightly west-dipping deposits of the lower parts (D1). These are composed of mainly well-bedded carbonates with a large-scale undulating lower boundary and small slumping structures. In contrast to Unit B with a general eastward-dipping direction (maximum inclination of 20°), the strata of Unit D1 dip to the west (maximum inclination of 10°). A few small-scale DFs with a maximum width of 20 m and a height of 2 m directly overlie Unit C (Fig. 5f) and, moreover, overlapping patterns are obvious. In section S6 a 2-m-thick stratified sand layer at the base of D1 disconformably overlies Unit B (Fig. 4); small bivalves are oriented horizontally in several layers of that carbonate-cemented sandstone.

At the western end of Unit D2, the lateral profile consists of poorly bedded to massive carbonates clearly Overlapping a debris flow from west to east

(Fig. 5g). East to this debris flow, a 25-m-wide, poorly exposed area was mapped, followed by a 40 m wide unit (ld 90 m) of a slump to debris flow, exhibiting both partly stratified beds and true DF deposits. Within the next 70 m (LD 150 m), poorly bedded nodular limestones occur dipping to the east with an inclination of 10° (Fig. 5j). Onlapping patterns are discernible where these poorly bedded layers overlie a 50-m-wide true DF, laterally grading into a slump to DF unit of 70 m width. Further to the east (LD 300 m), another 30-m-wide DF continues. Fine gravel covers Unit D2 in the eastern parts of the profile, where prevailing bedded strata have been discerned. At the easternmost end of the lateral profile, again a small DF has been mapped, unconformably overlain by bedded nodular limestones of Unit F (Fig. 5l). Similar to Unit B *Thalassinoides* burrows were found at the top. Carbonates of Unit D1 reflect deeper shelf to shallow slope deposits, compared with hemipelagic drape deposits on slopes (Prather et al. 1998). The intercalated sandstone layer (section S6) reflects a discontinuous channelised body that has been interpreted as sediment derived from submarine canyons. Unit D2 comprises all lateral and vertical transitions from slumps to DFs. A clear separation between them is not always possible (see discussion for Unit B).

Unit E

Unit E (thickness 20–40 cm) unconformably overlying Unit D consists of a thin chalk-marl couplet. It could be traced from east to west throughout the entire profile and was also identified in section S9 (Fig. 1).

Unit F

Unit F (thickness 10–12 m) could not be mapped in detail neither in the field nor with the photo-mosaic because of the poor exposure and strong weathering of this topmost Unit F. Two macroscopically determined facies have been distinguished: bedded carbonates and DFs. The DFs of Unit F consist mainly of clasts with only little surrounding matrix, in contrast to the DFs from the lower units (B and D) with a minor volume of clasts. Few of the bedded carbonates show internally nodular structures. In section S1 the overlying Unit F is composed of a small debris flow with single to few clasts (Fig. 5e), here with a clearly visible erosive contact between them.

Whereas the debris flows of Unit F exhibit a plastic internal mechanical behaviour, the nodular limestones argue for an elastic behaviour formed within translational slides (glides sensu Cook and Mullins 1983).

Microfacies types (MFT)

In Table 1 the important components are listed and their distribution within the microfacies types is marked. Figure 6 shows the microfacies-type distribution throughout sections S1–S8 with stratigraphic correlation.

MFT1 Planktic foraminifers micrite

It was formed as hemipelagic mud in deeper shelf areas, not or only slightly influenced by nearby shallow-water deposits. The relatively high quartz content may be derived from submarine canyons and reflects sediment bypassing (Fig. 7).

MFT2 Micrite with quartz

The co-occurrence of planktic foraminifers, filaments, and further small bioclasts in MFT2 combined with the absence of shallow-water biota is interpreted as being characteristic of outer ramp environments, again influenced by siliciclastic sediment bypassing.

MFT3 *Discocyclina* micrite

Bryan (1991) described *Discocyclina* from deep fore-reef and upper-basin slope environments similarly to Ghose (1977), who described long, flat *Discocyclina* from the fore-reef. Gietl (1998) reported *Discocylina* from the middle-ramp facies of the Galala areas. MFT3 was attributed to autochthonous middle- to outer-ramp environments because of the abundance of long, flat *Discocyclina* and *Asterocyclina* and the small quantity of other biota.

MFT4 Micritic sandstone

The quartz grains are derived from siliciclastic shoals of the shallow ramp (Gietl 1998). We interpret their occurrence in section S6 as a result of transportation downslope via submarine canyons. An amalgamation with DFs cannot be excluded due to their similarities to MFT2.

MFT5 Corallinacean nummulitid micrite to sparite

The coralline algae can be used for palaeobathymetric interpretations. According to Bosence (1991) small solitary and branching forms occur in medium energy reefs and buildups such as marl or back-reef mounds. Autochthonous floatstones with coralline algae have been described by Gietl (1998) from upper Paleocene
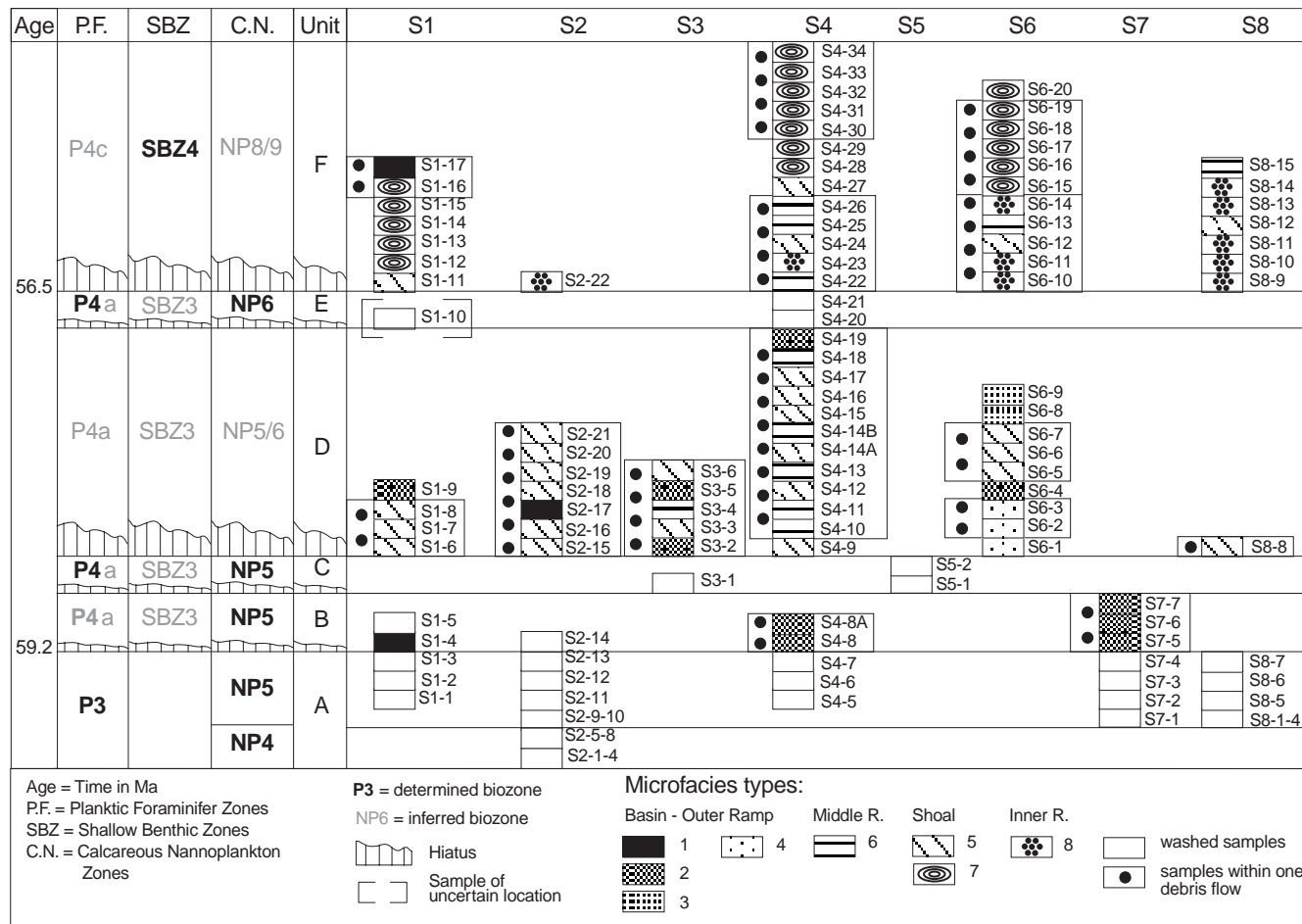
Fig. 6 Microfacies-type distribution throughout sections S1–S8 with stratigraphic correlation. The samples grouped together with *dots* are from one DF. Note that the debris flows are often formed by only one microfacies type

Legend (Fig. 6):

Age = Time in Ma
P.F. = Planktic Foraminifer Zones
SBZ = Shallow Benthic Zones
C.N. = Calcareous Nannoplankton Zones

P3 = determined biozone
NP6 = inferred biozone
Hiatus
Sample of uncertain location

Microfacies types:

Basin - Outer Ramp: 1, 2, 3, 4
Middle R.: 6
Shoal: 5, 7
Inner R.: 8
washed samples
samples within one debris flow

Table 1 Distribution of components in the MF types

MF-types	number of thinsections	Dunham-Classification	components	micrite	sparite	planktic foraminifers	discocyclinidae	nummulitidae	miscellanea	glomalveolina	conical foraminifers	miliolids	Hottingerina lukasi	coralline algae	corals	dasycladaceans	echinoderms	peloids	intraclasts	quartz	occurance:clast(c)/bed(b)	prevailing in unit	interpretation
1-Planktic foraminifers micrite	3	w	▮	▮	|	▮		|								|		|	▮	c,b	all	hemipelagic mud
2-Micrite with quartz	10	w,p	▮	▮	|	|		|								|		|	▮	c,b	B,D	outer ramp
3-Discocyclina micrite	2	w,p	▮	▮	|	|	▮							|		|		|		b	D	outer to middle ramp
4-Micritic sandstone	3	p	▮	▮	|	▮												|	▮	c,b	D	outer ramp
5-Corallinacean nummulitid micrite to sparite	26	p	▮	▮	▮		|	▮	▮		|	|	▮	|	|	|	▮	|	c,b	D,F	shoal, middle to inner ramp
6-Coral micrite	11	p	▮	▮	|		|	▮	|			|	▮	▮	|	|	|		c,b	D,F	coral-algal reef
7-Nummulitid micrite to sparite	18	p	▮	▮	▮		|	▮	▮	|	|	|	|	|	|	▮	|	▮	c,b	F	nummulitid shoal, middle to inner ramp
8-Miliolid biopel sparite to micrite	10	p	▮	▮	▮		|	|	|	|	▮	|	|	|	|	|	▮	|	c,b	F	inner ramp

— rare   ▬ common   ▮ abundant   ■ very abundant

limestones of the North Galala, where they occur in deeper environments of the inner ramp. This interpretation is in good concordance with observations by Buchbinder (1977) who described similar algal deposits of Miocene back-reef platform areas in Israel.

MFT6 Coral micrite

The allochthonous coral fragments dominate MFT6 which was originally formed as talus of coral algal reefs, although a reef belt has not been reported by previous authors from the areas further north. Our observations suggest at least broader patch reefs. Similar small-scale Early Paleocene coral algal reefs have been reported by, for example, Vecsei and Moussavian (1997) from the Maiella Platform (Italy) and Schuster (1996) from the Abu Tartur Plateau (western Egypt).

MFT7 Nummulitid micrite to sparite

The limestones of MFT 7 were originally formed close to nummulitic shoal environments situated near inner to middle ramp positions (Gietl 1998). Allochthonous alveolinids and dasycladaceans demonstrate inner-ramp influences. The two subtypes reflect no true nummulitid shoal deposits as described by Gietl (1998) but are deposited in back- or fore-shoal areas.

MFT8 Miliolid biopel sparite to micrite

This MFT reflects inner-ramp environments and includes reworked particles from restricted areas, documented by the high amounts of miliolids and endolithic algae. This is also indicated by the occurrence of conical imperforate foraminifers (Hottinger and Drobne 1980). The high content of nummulitids is interpreted as a result of redeposition.

Discussion

The lateral and vertical distribution of the studied late Paleocene sediments allowed reconstruction of the sedimentation processes of a ramp-to-basin transition during seven successive stages (Fig. 8A–F). On the basis of all sedimentological and stratigraphic data, the progradation of mainly allochthonous carbonate ramp deposits (of outer-mid ramp to mid-shallow ramp origin) and their interfingering with autochthonous basin sediments is illustrated.
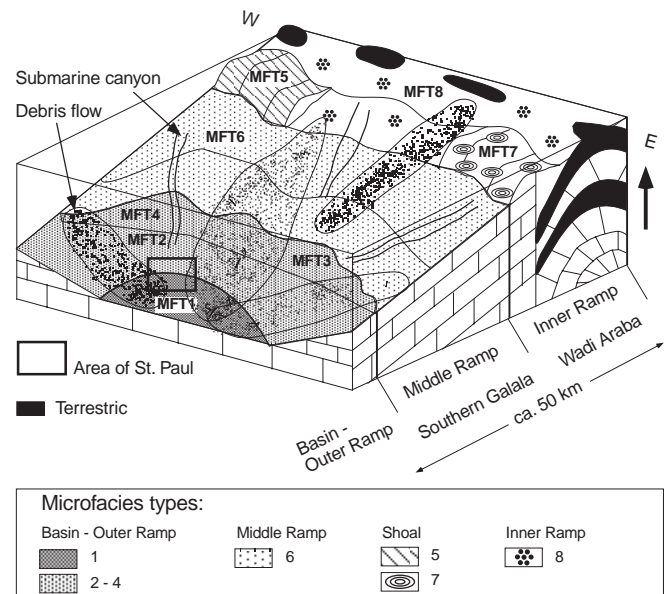
Fig. 7 Model of the southward-dipping ramp of the Galala Mountains. Microfacies-type distribution is inferred from the DFs of the investigated lateral profile by the monastery of St. Paul

Types of mass transport

The main transport mechanisms of the sediments described here are mass-transport processes due to gravity forces. Einsele (1991) summarized many descriptions of prevailing siliciclastic mass-transport deposits. Carbonate-dominated mass-transport processes have been subdivided by Cook and Mullins (1983) into three types: rockfall, slides and sediment gravity flows (Table 2). Slides can furthermore be divided into translational (glide) and rotational (slump) types. The shear plane of glides is parallel to the underlying beds, whereas in slumps the shear planes are concave-upward with a backward rotation of the slumped body (Cook and Mullins 1983). Middleton and Hampton (1976) defined the term sediment gravity flow as "flows consisting of sediment moving downslope under the action of gravity". They distinguished four subtypes that differ in the support mechanisms of the single grains within the flow: debris flow, grain flow, fluidized sediment flow and turbidity current. Lowe (1976) added the liquefied sediment flow to these four subtypes. These classifications represent idealized members of sediment gravity flows, and real flows can show all transitions between the grain support mechanisms (Middleton and Hampton 1976). Along a lateral transect, one subtype may also induce the other, e.g. a glide may induce a DF which itself could induce a turbidity current. Thus, they might evolve during downslope transport, when the rheological (Prior and Coleman 1984) or relief parameters (Piper et al. 1999) change. Within the gravity flow processes, DFs (cohesive) and turbidites are the

Table 2 Major types of submarine mass transport on slopes and their transport mechanism and dominant sediment support. (Modified after Cook and Mullins 1983)

Types of mass transport		Transport mechanism and dominant sediment support
Rockfall		Freefall and rolling single blocks along steep slopes
Slide	translational (Glide)	Shear failure along discrete shear planes subparalell to underlying bed
	rotational (Slump)	Shear failure along discrete concave-up shear planes accompanied by rotation of slide
Sediment gravity flow	Debris flow or Mud flow	Shear distributed throughout the sediment mass. Clasts supported above base of bed by cohesive strength of mud matrix and clast buoyancy. Can be initiated and move long distances along very low angle slopes
	Grain flow	Cohesionless sediment supported by dispersive pressure. Usually requires steep slopes for initiation and sustained downslope movement
	Liquefied flow	Cohesionless sediment supported by upward displacement of fluid. Requires slopes > 3°
	Fluidized flow	Cohesionless sediment supported by upward motion of escaping pore fluid. Thin and short lived
	Turbidity current flow	Clasts supported by fluid turbulence. Can move long distances along low angle slopes

main mechanisms for sediment transport (Mutti 1992), whereas the others, such as grain flows, liquefied flows and fluidized flows, represent transient conditions that occur within gravity flows during transport. Further details about flow regimes in sediment gravity flows are found in Postma (1986), Fisher (1983), Enos (1977) and Einsele (1991). In the lateral profile studied, slides (represented by glides and slumps) and sediment gravity flows (represented by DF) including transitions between both are most frequent.

Debris flow deposits

Debris flow deposits vary in size and shape, both vertically and horizontally. Moreover, they contain different types of clasts also varying in size. The following short description summarizes major differences of DFs observed macroscopically.

All DFs vary in thickness between 0.5 and 7 m and in width between 10 and 50 m; however, originally greater thickness values may have been reduced by subsequent erosion. The most common DF shape is represented by convex-upward lenses often visible only at one side of a DF cross section (Figs. 5f,g,j,l; see also Mutti 1992) with onlap patterns of the younger sediments. Few DFs exhibit convex-downward shapes (Fig. 5d) with sharp contacts to the overlying layers. Sharp straight contacts can also be seen in convex-upward DFs, especially the large ones of Unit D which are directly overlain by Unit E (Fig. 4). This contact is probably an erosional feature (Fig. 5j).

Two main groups of DFs have been distinguished: matrix supported (DF 1) and clast supported (DF 2). Within the first containing well-sorted clasts (all within a fine matrix), two different subtypes have been established (DF 1a, b) ranging from small clasts
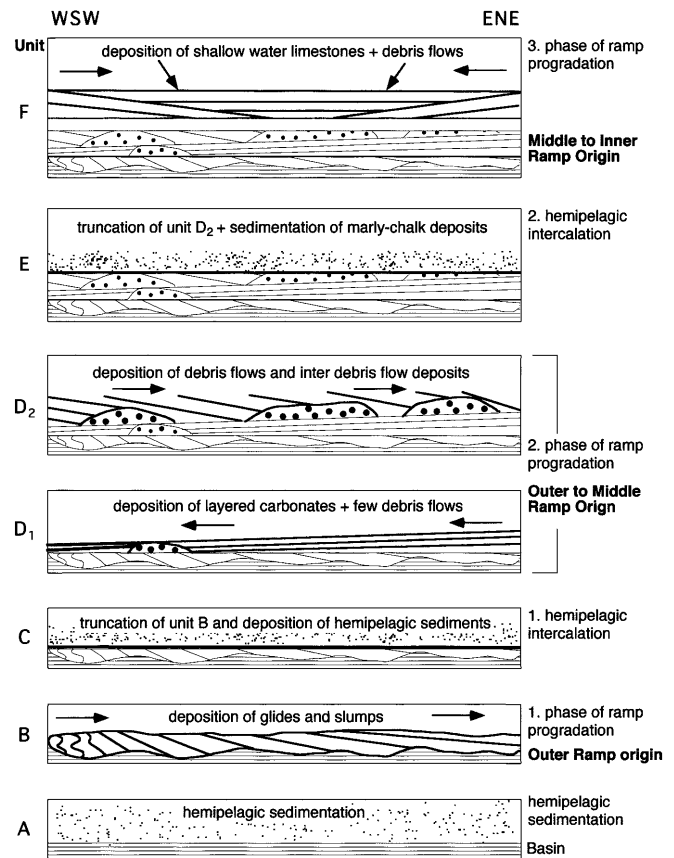
Fig. 8 Deposition mode of the units indicating the different phases of ramp progradation and location of deposition. Unit A: hemipelagic sedimentation. Unit B: first phase of ramp progradation with deposition of glides and slumps from westerly directions; samples indicate an outer-ramp origin. Unit C: truncation of Unit B and first hemipelagic intercalation. Unit D1: second phase of ramp progradation with deposition of layered carbonates and few DFs from easterly directions. Unit D2: deposition of DFs and inter-DF sediments from westerly directions; samples of Unit D indicate an outer- to middle-ramp origin. Unit E: truncation of Unit D2 and second hemipelagic intercalation. Unit F: third phase of ramp progradation with deposition of shallow-water limestones and DFs from all directions except the south; samples indicate a middle- to inner-ramp origin

with a maximum diameter of 1 cm (DF 1a; Fig. 5a) to large clasts of 25–50 cm diameter (DF 1b; Fig. 5c). Both subtypes of well-sorted DFs are found only in the vicinity of section S8, whereas all the other matrix-supported DF deposits are characterised by a lesser sorting of clasts (Fig. 5b). Thirty-three clasts of DF-1 deposits have been sampled for the detailed descriptions of MFTs given previously. We selected fossil-bearing clasts without macroscopically discernible diagenetic overprints. Therefore, the MFT distribution shown for the entire outcrop (Fig. 6) reflects a non-statistical distribution (over-representation). Micrites with planktic foraminifers (MFT1) are present in all DFs in varying amounts. Only few micritic samples were taken, resulting in an under-representation in Fig. 6.

Clast-supported DFs (DF 2) have been observed only in Unit F, often with transition to nodular limestones. This type of DF has little or no matrix, and in contrast to DF 1, all 22 clast samples taken contain mainly fossil-bearing MFTs. Most DFs found are composed of only one MFT, e.g. Unit D2 of MFT5 or Unit F of MFT7 (Fig. 6).

Evolution of units

The upper Maastrichtian hemipelagic chalk-marl deposits of the area south of the South Galala continue in marly lower Paleocene sediments (Unit A). Whereas the stratigraphic succession of the lateral profile spans from zone P3 (NP4) upwards, the neighbouring section S9 (Fig. 1) spans an upper Maastrichtian–Paleocene succession. In section S9 zones P1–P4 and NP1–NP5 were encountered. Benthic foraminiferal assemblage, including *Gavelinella beccariformis* and *Nuttallides truempyi*, indicate "bathyal" deposition (R.P. Speijer, pers. commun.).

Unit B was formed during late NP5 times, but a short-term hiatus is indicated by the basal erosive contact with the underlying Unit A (Figs. 3, 4). The carbonates of Unit B originated from distal ramp settings and represent the first phase of early late Paleocene ramp progradation onto hemipelagic sediments. Here, glides and slumps are obvious (Fig. 5g to 5k), and even few small-scale DFs occur (Fig. 5l). Prevailing eastward-dipping directions of glides and slumps indicate a -west–east direction of transport (Fig. 8). We assume that these mass-transport deposits were formed in outer-ramp environments, as indicated by characteristic MFTs determined in clasts that were derived from the internal parts of DFs in sections S4 and S7.

Prior to the onset of Unit C, the carbonate sedimentation of Unit B ceases as evidenced by the occurrence of decimetres-thick *Thalassinoides* burrows at the top. Formed within aerobic environments (Zhicheng et al. 1997), these *Thalassinoides* burrows indicate a decrease of sedimentation rates during late Unit-B times and the top of the burrows may represent a flooding surface.

The soft hemipelagic marls of Unit C (NP5) disconformably overlie the limestones of Unit B. The benthic foraminifers show a mixture of autochthonous deeper (mixed Midway and Velasco Fauna) and allochthonous shallower shelf forms (Speijer 1994; R.P. Speijer, pers. commun.). Unit C was possibly deposited under rising sea-level conditions and marks the transgressive part of the sea-level curve.

The exact stratigraphic position of Unit D remains questionable: a latest NP5 or early NP6 age is possible, because Unit D is sandwiched between upper NP5 deposits of Unit C and NP6 deposits of unit E (Fig. 3). Sedimentologically, these carbonates represent the second phase of ramp progradation and

can be subdivided into a lower Unit D1 and an upper Unit D2. The first is composed of mainly well-bedded carbonates with onlap patterns towards the west onto Units B or C, clearly indicating transport directions from the east (Fig. 8D). Slumpings may occur (Fig. 5j) and few DFs are present (Fig. 5h). In contrast to the DFs of Unit B (where all clasts are composed of micrite with abundant quartz grains), DFs here contain clasts exhibiting various microfacies types. Those of section S2 consist of corallinacean-nummulitid micrite to sparite (MFT5) indicating shallow-water shoal deposition of the inner to middle ramp. In contrast, DFs (and also the well-bedded carbonates) of section S6 are dominated by micritic sandstones, whereas all other bedded sediments of Unit D1 are composed of micrite-dominated limestones without fossils. We interpret the siliciclastic layer as being transported via submarine canyons that cut through the slope transect and thus reflect siliciclastic sediment bypassing (Fig. 7). An amalgamation of these with various facies types originally formed in different ramp environments has been assumed. Similarities of D1 limestones to those of Unit B are obvious, both originally deposited at the outer ramp. The first, however, exhibits a stronger influence of shallow-water deposition.

The upper Unit D2 is characterised by large-scale DFs and slump to DF deposits with inter-debris flow deposits of weakly stratified nodular limestones (section S3; Fig. 4). Most clasts of the DFs here represent deposits of the middle to inner ramp, which originally consisted of mainly corallinacean-dominated microfacies types with abundant nummulitids. In contrast to Units D1 and B, bedded limestones with deep-water microfacies types are rarely present. The quartz content of these sediments is low. Because of dominating shallow-water MFTs, a more proximal outer- to middle-ramp position is proposed. Only the nodular limestones of section S3 indicate transport directions from west to east, whereas DFs and slump to DF deposits exhibit no transport directions. Similar to unit B, sedimentation on top of Unit D ceased, as documented by *Thalassinoides* burrows (section S6), and subsequent erosion occurred. This may represent a flooding surface. The DFs and slump to DF deposits are here truncated at the top. Usually, DFs are characterised by convex-upward shapes (Mutti 1992), but this feature was observed only at their sides, whereas their tops end with sharp contacts towards the overlying Unit E.

The marly chalky sediments of Unit E in all sections disconformably overlie the limestones of Unit D (Fig. 5e). Unit E represents a second short intercalation of hemipelagic basinal sediments formed during an interval when the export of carbonates from the ramp was interrupted by rising sea-level conditions. Similar to Unit C this marks the transgressive part of the sea-level curve. Nannofossils indicate a late Paleocene age of biozone NP6; however, the duration of

the hiatus at the disconformable boundary to Unit D below cannot be estimated. The exact position of the NP5–NP6 boundary is within Unit D or the hiatus thereafter (Fig. 3). The hiatus-surface at the top of Unit E separates shallow-water deposits of the mid to inner ramp (Unit F) from hemipelagic marls of Unit E. Similar to Unit C benthic foraminifers show a mixture of autochthonous deeper (mixed Midway and Velasco Fauna) and allochthonous shallower shelf forms (Speijer 1994; R.P. Speijer, pers. commun.). Small larger foraminifers were found as well (R.P. Speijer, pers. commun.).

Unit F has been assigned to SBZ4. According to the shallow benthic zonation (Fig. 3) given by Serra-Kiel (1998), these sediments have been correlated with the plankton/nannoplankton chronology of Berggren et al. (1995) and Martini (1971) and correlate to P4c/NP8/9. Unit F represents the third phase of ramp progradation characterised by small-scale DFs and nodular limestones (without distinct stratification), and both lithofacies are often hard to differentiate. Similar to Units B and D, reworking of sediments originating from different facies zones was evident in Unit F, with prevailing shallow-water deposits from mid- to inner-ramp settings. Imprints of the shallowest inner ramp deposits (miliolid biopel sparite to micrite) are observed. In contrast to the shoal deposits of Unit D (composed of corallinacean-nummulitid micrite to sparite), nummulitid micrite to sparite prevail here. As indicated in Fig. 8F, no dominant transport direction occurs: dipping directions vary from west, south to east, suggesting a general southward-directed transport. The deposits of Unit F reflect middle- to inner-ramp environments.

Sea level as trigger mechanism for mass-transport deposition

The two factors responsible for initiation of mass transports are strength reduction and stress increase (Prior and Coleman 1984). Strength reduction is essentially a product of internal sediment variations of water content, pore water and gas pressure. They can be changed by sedimentary loading, pressure from surface waves during storms, sea-level changes, and pore-gas generation due to internal geochemical and bacteriological processes. A gravitational stress increase might be induced by tectonics, localized sea-floor erosion, waves and sedimentation (Prior and Coleman 1984). Debris flows are deposited when the gravitational force decreases below the strength of the debris and a sudden "freezing" occurs (Middleton and Hampton 1976).

Among the various factors and mechanisms that control the slope sedimentation, we discuss the mass-transport deposits of St. Paul in light of fluctuations of the relative sea level that may influence accommodation space at the ramp: sea-level drops initiate ramp progradation. Recent studies on the Paleocene sea-level history of the Sinai (Lüning et al. 1998) suggest a main sea-level drop at the base of P4 (within NP5) and subsequent sea-level oscillations during P4, similar to the cycle boundaries of Hardenbol et al. (1998). Speijer and Schmitz (1998) reconstructed a paleao-depth curve of that interval based on studies of benthic foraminifers from Gebel Aweina (ca. 300 km to the south). These authors also concluded a sea-level drop during lower P4 (upper part of NP5), matching TH 1 of Hardenbol et al. (1998) and probably TH Sin2 of Lüning et al. (1998). If the mass-transport deposits of Units B and D and the respective cycle boundaries SelGal2 and SelGal(?) would be considered as lowstand deposits, this would fit in the sequence stratigraphic frame of Lüning et al. (1998) and Hardenbol et al. (1998); however, if both mass-transport deposits would be attributed to the same sea-level lowstand, the duration of Unit C would be very short. Another possibility is the non-correlation of one of the two cycle boundaries with any known lowstand. This might have two reasons: the local character of the lowstand, or mass-transport deposits of one of the units are not related to a sea-level lowstand but are triggered by other mechanisms, e.g. tectonics. However, the onset of the mass-transport deposits of unit F (due to ramp progradation and regional lowstand) coincides with cycle boundary ThGal1 (Fig. 3), as per TH Sin5 (Lüning et al. 1998) and TH 4 (Hardenbol et al. 1998) and a sea-level drop discussed by Speijer and Schmitz (1998).

Conclusion

During the late Paleocene (P3–P4) interval, three phases of carbonate ramp progradation and three hemipelagic units were differentiated at the southern Galala (St. Paul). The three prograding phases are indicated by increased mass-transport deposition composed of glides, slumps and DFs which came from different directions excluding the south. Each subsequent advance of ramp progradation was more pronounced. Microfacies investigations (deduced mainly from clasts in the DF deposits) highlight the changing depositional origins from a basinal outer-ramp setting to a middle- to inner-ramp setting at the end of the Paleocene. Moreover, changes in organism composition with time were evidenced: During early P4, corallinacean algae thrived on the ramp (especially at the inner- to middle-ramp transition and the shoal area), whereas during late P4 these areas were dominated by nummulitids.

Sea-level changes are a likely trigger for the onset of mass-transport deposition. Comparisons with regional cycle boundary interpretations led to the attribution of at least two mass-transport deposits to lowstands. The two older mass transport deposits (Units B and D) either reflect one event (attributed

to a single sea-level drop) or one of them reflects a local lowstand or has been triggered by other mechanisms independent of sea-level change, e.g. tectonics. Both, Units B and D, show on top of the strata abundant *Thalassinoides* burrows followed by hemipelagic marly intercalations that are probably indications for a flooding surface indicating a subsequent transgressive phase.

In contrast to the carbonate mass-transport deposits, siliciclastic sediments are of minor importance in the investigated area. They are probably sourced via submarine canyons and reflect sediment bypassing. Whereas the transport mechanism of siliciclastic deposits has a point-source character, carbonate deposits are dominated by a line-source character.

References

Abdel-Kireem MR, Abdou HF (1979) Upper Cretaceous–Lower Tertiary planktonic foraminifera from South Galala Plateau, Eastern Desert, Egypt. Rev Espanola Micropaleontol 11:175–222

Abdou HF, Naim EM, Sultan IZ (1969) Biostratigraphic studies on the Lower Tertiary rocks of Gebel Umm Rokham and Saint Paul area, Eastern Desert, Egypt. Bull Faculty Sci Alexandria 9:271–299

Aigner T (1983) Facies and origin of nummulitic buildups: an example from the Giza Pyramids Plateau (Middle Eocene, Egypt). N Jahr Geol Paläont Abh 166:347–368

Bandel K, Kuss J (1987) Depositional environment of the pre-rift sediments: Galala Heights (Gulf of Suez, Egypt). Berliner Geowiss Abh A 78:1–48

Berggren WA, Kent DV, Swisher CC III, Aubry MP (1995) A revised Cenozoic geochronology and chronostratigraphy. In: Berggren WA, Kent KV, Aubry MP, Hardenbol J (eds) Geochronolgy, time scales, and global stratigraphic correlation. SEPM Spec Publ 54:129–212

Bosence DWJ (1991) Coralline algae: mineralization, taxonomy, and palaeoecology. In: Riding R (ed) Calcareous algae and stromatolites. Springer, Berlin Heidelberg New York, pp 98–113

Bryan JR (1991) A Paleocene coral-algal-sponge reef from southwestern Alabama and the ecology of Early Tertiary reefs. Lethaia 24:423–438

Buchbinder B (1977) The coralline algae from the Miocene Ziqlag Formation in Israel and their environmental significance. In: Flügel E (eds) Fossil algae: recent results and developments. Springer, Berlin Heidelberg New York, 279–285

Cook HE, Mullins HT (1983) Basin margin environment. In: Scholle PA, Bebout DG, Moore CH (eds) Carbonate depositional environments. AAPG Mem 33:539–617

Drobne K (1975) *Hottingerina lukasi* n.gen., n.sp. (Foraminiferida) iz srednjega paleocena v severozahodni jugoslaviji. Radzprave 18:242–253

Einsele G (1991) Submarine mass flow deposits and turbidites. In: Einsele G, Ricken W, Seilacher A (eds) Cycles and events in stratigraphy. Springer, Berlin Heidelberg New York, pp 313–339

Enos P (1977) Flow regimes in debris flow. Sedimentology 24:133–142

Faris M (1995) Late Cretaceous and Paleocene calcareous nannofossil biostratigraphy at St. Paul section, southern Galala Plateau, Egypt. Ann Geol Surv Egypt 20:527–538

Fisher RV (1983) Flow transformations in sediment gravity flows. Geology 11:273–274

Ghose BK (1977) Paleoecology of the Cenozoic reefal foraminifers and algae: a brief review. Palaeogeogr Palaeoclimatol Palaeoecol 22:231–356

Gietl R (1998) Biostratigraphie und Sedimentationsmuster einer nordostägyptischen Karbonatrampe unter Berücksichtigung der Alveolinen-Faunen. Berichte Fachbereich Geowiss Univ Bremen 112:1–135

Hardenbol J, Thierry J, Farley MB, Jacquin T, Graciansky PC de, Vail PR (1998) Mesozoic–Cenozoic sequence chronostratigraphic framework of European basins. In: Graciansky PC de, Hardenbol J, Jacquin T, Vail PR, Farley MB (eds) Sequence stratigraphy of European basins. SEPM Spec Publ 60:1–13

Hottinger L, Drobne K (1980) Early Tertiary conical imperforate foraminifera. Radzprave 22:188–276

Hottinger L, Lehmann R, Schaub H (1964) Donèes actuelles sur la biostratigraphie du Nummulitique Méditerranéen. Mém Bur Rech Geol Min (Colloque Paléogène, Bordeaux) 28:611–652

Ismail MM, Abdallah AM (1966) Contribution to the stratigraphy of St. Paul Monastery area by microfacies. Bull Faculty Sci Alexandria 12:325–334

Kulbrok F (1996) Biostratigraphie, Fazies und Sequenzstratigraphie einer Karbonatrampe in den Schichten der Oberkreide und des Alttertiärs Nordost-Ägyptens (Eastern Desert, N'Golf von Suez, Sinai). Berichte Fachbereich Geowiss Univ Bremen 81:1–216

Kulbrok F, Kuss J (1995) Sedimentary sequences of the Late Cretaceous/early Tertiary succession in NE Egypt. Terra Nostra 1:28–29

Kuss J, Leppig U (1989) The early Tertiary (middle-late Paleocene) limestones from the western Gulf of Suez, Egypt. N Jahrb Geol Paläont Abh 177:289–332

Kuss J, Scheibner C, Gietl R (submitted) Late Cretaceous-early Tertiary platform to basin transition along a Syrian Arc uplift (Eastern Desert, Egypt)

Leppig U (1987) Biostratigraphy of larger foraminifera and facies development from the Upper Albian to the Middle Paleocene in the Sierra de Cantabria and the Montes Obarenes (northwestern Spain). N Jahrb Geol Paläont Mh 1987:647–666

Lowe DR (1976) Subaqueous liquefied and fluidized sediment flows and their deposits. Sedimentology 23:285–308

Luger P (1985) Stratigraphie der marinen Oberkreide und des Alttertiärs im südwestlichen Obernil-Becken (SW-Ägypten) unter besonderer Berücksichtigung der Mikropaläontologie, Palökologie Paläogeographie. Berliner Geowiss Abh A 63:1–151

Lüning S, Marzouk AM, Kuss J (1998) The Paleocene of central East Sinai, Egypt: "sequence stratigraphy" in monotonous hemipelagites. J Foraminiferal Res 28:19–39

Martini E (1971) Standard Tertiary and Quaternary calcareous nannoplankton zonation. In: Farinacci A (ed) Proc Second Planktonic Conference, Rome 1970, pp 739–785

724

Middleton GV, Hampton MA (1976) Subaqueous sediment transport and deposition by sediment gravity flows. In: Stanley DJ, Swift DJP (eds) Marine sediment transport and environmental management. Wiley, New York, pp 197–218

Moustafa AR, Khalil MH (1995) Superposed deformation in the northern Suez Rift, Egypt: relevance to hydrocarbons exploration. J Petrol Geol 18:245–266

Mutti E (1992) Turbidite sandstones. Agip S.p.A., Milan, pp 1–275

Olsson RK, Hemleben C, Berggren WA, Huber BT (1999) Atlas of Paleocene planktonic foraminifera. Smithsonian Institution Press, Washington DC, pp 1–252

Piper DJW, Cochonat P, Morrison ML (1999) The sequence of events around the epicentre of the 1929 Grand Banks earthquake: initiation of debris flows and turbidity current inferred from sidescan sonar. Sedimentology 46:79–97

Postma G (1986) Classification for sediment gravity-flow deposits based on flow conditions during sedimentation. Geology 14:291–294

Prather BE, Booth JR, Steffens GS, Craig PA (1998) Classification, lithologic calibration, and stratigraphic succession of seismic facies of intraslope basins, deep-water Gulf of Mexico. AAPG Bull 82:701–728

Prior DB, Coleman JM (1984) Submarine slope instability. In: Brunsden D, Prior DB (eds) Slope instability. Wiley, New York, pp 419–455

Schuster F (1996) Paleoecology of Paleocene and Eocene corals from the Kharga and Farafra Oases (Western Desert, Egypt) and the depositional history of the Paleocene Abu Tartur carbonate platform, Kharga Oasis. Tübinger Geowiss Arbeit A 31:pp 1–96

Serra-Kiel J, Hottinger L, Caus E, Drobne K, Ferrandez C, Jauhri AK, Less G, Pavlovec R, Pignatti J, Samso JM, Schaub H, Sirel E, Strougo A, Tambareau Y, Tosquella J, Zakrevskaya E (1998) Larger foraminiferal biostratigraphy of the Tethyan Paleocene and Eocene. Bull Soc Géol France 169:281–299

Speijer RP (1994) The late Paleocene benthic foraminiferal extinction as observed in the Middle East. Bull Soc Belge Géol 103:267–280

Speijer RP, Schmitz B (1998) A benthic foraminiferal record of Paleocene sea level and trophic/redox conditions at Gebel Aweina, Egypt. Palaeogeogr Palaeoclimatol Palaeoecol 137:79–101

Strougo A, Haggag MAY, Luterbacher H (1992) The basal Paleocene "*Globigerina*" *eugubina* zone in the Eastern Desert (St. Paul's Monastery, South Galala), Egypt. N Jahrb Geol Paläont Mh 1992:97–101

Vecsei A, Moussavian E (1997) Paleocene Reefs on the Maiella platform margin, Italy: an example of the effects of the Cretaceous/Tertiary boundary events on reefs and carbonate platforms. Facies 36:123–140

White MR (1994) Foraminiferal biozonation of the northern Oman Tertiary carbonate succession. In: Simmons MD (eds) Micropaleontology and hydrocarbon exploration in the Middle East. Chapman and Hall, London, pp 309–332

Zhicheng Z, Willems H, Binggao Z (1997) Marine Cretaceous–Paleogene biofacies and ichnofacies in southern Tibet, China, and their sedimentary significance. Mar Micropaleontol 32:2–3